Earth Surface Processes and Landforms
Earth Surf. Process. Landforms **30**, 325–338 (2005)
Published online in Wiley InterScience (www.interscience.wiley.com). **DOI:** 10.1002/esp.1144

Simulated effect of a forest road on near-surface hydrologic response and slope stability

Anona L. Dutton[1], Keith Loague[2,*] and Beverley C. Wemple[3]
[1] *Erler and Kalinowski, Inc., 1870 Ogden Drive, Burlingame, CA 94010, USA*
[2] *Department of Geological and Environmental Sciences, Stanford University, Stanford, CA 94305-2115, USA*
[3] *Department of Geography, University of Vermont, Burlington, VT 05405-4170, USA*

**Correspondence to: K. Loague, Department of Geological and Environmental Sciences, Stanford University, Stanford, CA 94305-2115, USA. E-mail: keith@pangea.stanford.edu*

Received 29 October 2003;
Revised 21 May 2004;
Accepted 19 July 2004

Abstract

Forest management practices often result in significant changes to hydrologic and geomorphic responses at or near the earth's surface. A well-known, but not fully tested, hypothesis in hillslope hydrology/geomorphology is that a near-surface permeability contrast, caused by the surface compaction associated with forest roads, can result in diverted subsurface flow paths that produce increased up-slope pore pressures and slope failure. The forest road focused on in this study is located in a steep forested, zero-order catchment within the H. J. Andrews Experimental Forest (Oregon). A three-phase modelling effort was employed to test the aforementioned hypothesis: (i) two-dimensional (vertical slice), steady-state, heterogeneous, saturated subsurface flow simulations at the watershed scale for establishing the boundary conditions for the catchment-scale boundary-value problem in (ii); (ii) two-dimensional (vertical slice), transient, heterogeneous, variably saturated subsurface flow simulations at the catchment scale for estimating near-surface hydrologic response and pore pressure distributions; and (iii) slope stability analyses, using the infinite slope approach, driven by the pore pressure distributions simulated in (ii), for assessing the impact of the forest road. Both observed and hypothetical rainfall events are used to drive the catchment-scale simulations. The results reported here support the hypothesis that a forest road can have an effect on slope stability. The permeability contrast associated with the forest road in this study led to a simulated altering of slope-parallel subsurface flow with increased pore pressures up-slope of the road and, for a large rainfall event, a slope failure prediction.

Keywords: slope stability; forest roads; surface hydrologic response; subsurface flow; forest management

Introduction

Forest roads are an integral part of large scale logging operations. Much of what is known about the effect of forest roads appears to be intuitive. For example, related to hydrologic response, forest roads: (i) reduce infiltration, (ii) capture and channelize surface runoff, and (iii) modify subsurface flow paths. Much of the early work that considered forest roads was designed to assess the impact of forest management practices (e.g. Brown and Krygier, 1971; Harr *et al*., 1975; Beschta, 1978; Ziemer, 1981; Megahan and Clayton, 1983; King and Tennyson, 1984; Reid and Dunne, 1984; Bilby *et al*., 1989). In recent years there has been considerable interest in the forest road problem; for example, a special issue of *Earth Surface Processes and Landforms* was devoted to the hydrologic and geomorphic effects of forest roads (Luce and Wemple, 2000).

The simulation-based efforts summarized in Table I each consider the effects forest roads have on surface and/or near-surface hydrologic response. The difference between the effort reported herein and most of the other studies summarized in Table I is that the focus is on subsurface pore pressure development versus surface and/or near-surface discharge. Fisher (2000), the only other entry in Table I focused on subsurface pore pressure development, employed SUTRA for a swale in the Caspar Creek watershed. Dhakal *et al*. (2000) employed a combined surface/subsurface kinematic wave model to estimate groundwater levels, which are in turn used to drive slope stability analyses. Both Reid and Dunne (1984) and Ziegler *et al*. (2001) used simulated hydrologic response to drive estimates of

Table I. Selected hydrologic-response simulation studies where forest road impacts were considered

Reference	Scale*	Simulated hydrologic-response		Hydrologically driven assessment	
		Model type†	Process representation‡	Erosion	Slope stability
Reid and Dunne (1984)	W	E	O	✓	
Luce and Cundy (1994)	P	QPB	O		
Dhakal *et al.* (2000)	C	QPB	O, S		✓
Fisher (2000)	C	PB	S		
Ziegler *et al.* (2001)	P	QPB	O	✓	
Bowling and Lettenmaier (2001)	W	QPB/E	O, S		
Tague and Band (2001)	W	QPB/E	O, S		
Wigmosta and Perkins (2001)	W	QPB/E	O, S		
Wemple and Jones (2003)	C	E	O, S		
This study	C	PB	S		✓

* C, catchment; P, plot; W, watershed.

† E, empirical model; operating algorithms are not directly based on the partial-differential equations describing surface and/or subsurface flow; PB, Physically based model; employs numerical solution to the partial-differential equations describing surface and/or subsurface flow; QPB, quasi-physically based model; employs analytical solutions (as operating algorithms) to the partial-differential equations describing surface and/or subsurface flow.

‡ O, Overland flow; S, subsurface discharge.

transport-limited erosion. Reid and Dunne (1984) used unit hydrographs and sediment rating curves to describe sediment production rates from forest road surfaces. Ziegler *et al*. (2001) used KINEROS2 to estimate Horton overland flow and erosion from unpaved mountain roads. For the remaining entries in Table I hydrologic response was simulated with: a reduced infiltration capacity model similar to KINEROS2 (Luce and Cundy, 1994), DHSVM (Bowling and Lettenmaier, 2001; Wigmosta and Perkins, 2001), RHESSys (Tague and Band, 2001), and the Beven (1982) model for kinematic subsurface stormflow (Wemple and Jones, 2003).

The convergent and steeply sloping hollows typical of forested catchments are often filled with colluvium. These near-surface materials can have a significantly greater permeability than the underlying bedrock. The permeability contrast at the colluvium–bedrock interface can impede fluid flow and be conducive to the formation of locally elevated pore pressures (e.g. Rulon *et al*., 1985; Reid, 1997). Depending on the colluvium thickness, the permeability contrast, the degree of saturation, and the intensity of a given rainfall event, periodic slope failures can be triggered. The study by Rulon *et al*. (1985) combined two-dimensional (2D) variably saturated subsurface flow simulations with sandbox experiments to explore the link between permeability contrasts in layered hillslopes and the creation of perched water tables and multiple seepage faces. Rulon *et al*. (1985) found that the hydraulic head distribution and the subsurface flow discharged across the seepage face were highly dependent on the rainfall rate, the location and geometry of an impeding layer, and the magnitude of the permeability contrast. It should be pointed out that the compaction associated with a forest road often results in a near-surface permeability contrast.

The effort reported here is the foundation step of an ongoing study designed to develop a process-based understanding of the relationships between forest roads, surface and near-surface hydrologic response, and slope stability. The objective of this study was to quantitatively test the well-known hypothesis that a near-surface permeability contrast, caused by the surface compaction associated with forest roads, can result in diverted subsurface flow paths that produce increased up-slope pore pressures and slope failure. The work presented here is a simulation-based effort that focuses on a site within the H. J. Andrews Experimental Forest. To the best of our knowledge the effort reported here is the first to combine physics-based variably saturated subsurface flow with slope stability analysis for the forest road problem.

H. J. Andrews Experimental Forest

Background

In 1948 the US Forest Service established the Blue River Experimental Forest, renamed in *c*. 1953 to H. J. Andrews (HJA) Experimental Forest (see Figure 1a) to study the effects of logging and related forest management practices on watershed functions. The HJA encompasses the Lookout Creek watershed in the Western Cascades, approximately

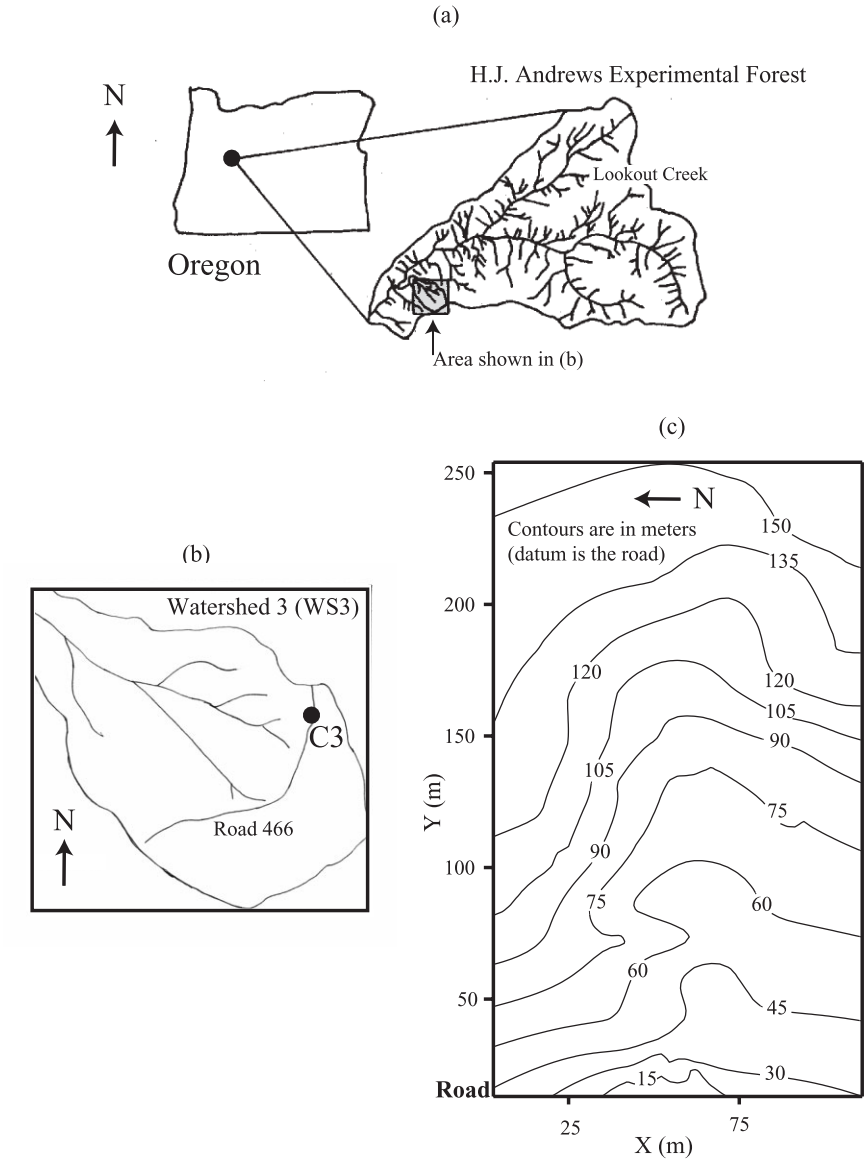

Figure 1. (a) H. J. Andrews Experimental Forest. (b) Location of WS3 and C3. (c) Topographic map for C3.

80 km east of Eugene, Oregon. In 1952 a long-term paired watershed study was initiated in the HJA to compare the effects of clearcutting (and the construction of forest roads) on hydrologic response and sedimentation. Over the past 50 years there has been considerable research conducted within the HJA (see http://www.fsl.orst.edu/lter/). Included within the 3024 publications listed on the HJA website is the lucid paper by Harr (1977) which describes near-surface water movement for forested soils.

The impact of forest roads within HJA is well documented. Analyses of long-term streamflow records have shown small but detectable increases in peak flows following road construction (Jones and Grant, 1996; Thomas and Megahan, 1998). This effect may be due to the interception of subsurface flow by roads (Wemple and Jones, 2003). Erosion inventories following extreme storm events have shown that roads account for a majority of mass movement events, despite occupying a small portion of the basin (Dyrness, 1967), and generate landslides at rates up to 30 times greater than in forested areas without roads (Swanson and Dyrness, 1975). More recent work indicates that the legacy of older road location and construction practices persists over time as roads on unstable slopes continue to be the most failure-prone during extreme storms (Wemple *et al*., 2001). Only one study at the HJA, which did not explicitly consider the effects of roads, has attempted to simulate the interplay between hydrology and slope stability (Duan, 1996).

Study area

Figure 1a and b show, respectively, the location of the HJA and the 1·0 km^2 Watershed 3 (WS3). Annual precipitation amounts for the HJA vary from 2·3 m in lower elevations to 3·6 m along the highest ridges (Jones and Grant, 1996). Overland flow is an uncommon occurrence on the unchannelled hillslopes of the HJA, except during extreme storm events. Seepage along the roadcuts in WS3 has been consistently observed during storms (Wemple and Jones, 2003). The catchment known as C3, located within WS3 (see Figure 1b), was the area of interest in this study. A 6-m wide forest road (established in 1959) dissects (side to side) the catchment. The 2 ha area of C3 shown in Figure 1c (located above the forest road, extending to the ridge-top) was the focus of the subsurface flow simulations and slope stability analyses reported herein. The C3 site was selected because of prior field study (see Wemple and Jones, 2003), concave topography, and sparse understorey vegetation.

New data for C3

The previously available information for C3 (see Wemple, 1998) included: geology, rainfall, and discharge. The field effort at C3 undertaken for this study (see Dutton, 2000) included a topographic survey and measurements of (i) soil depth, (ii) soil-water content, (iii) saturated hydraulic conductivity, and (iv) soil-water retention. The soil-water content measurements (at 35 locations) were made with time domain reflectometry. The saturated hydraulic conductivity measurements, in close proximity to the soil-water content measurements, for the surface and near-surface, were made, respectively, with a pressure infiltrometer and a Guelph permeameter. The soil-water retention curve was prepared based upon a series of field experiments (at three sites) consisting of successive and simultaneous soil-water content and pressure head measurements made (under irrigation) during infiltration.

Simulation Approach

The near-surface hydrologic response of C3 to rainfall events, in the form of 2D long profile (vertical slice), was used to quantitatively estimate pore pressures for slope stability analyses with consideration of the forest road. The long profile of interest in this study dissects (up-slope to down-slope) the area of interest. In that it was not feasible to conduct simulations of variably saturated flow for the entire WS3 boundary-value problem (BVP), the study was undertaken as a three-phase effort. In Phase I, the C3 BVP was gleaned from regional-scale simulations of saturated steady-state subsurface flow for WS3. Specifically, the Phase I simulations facilitated a quantitative characterization of the C3 subsurface flow system by establishing the dimensions and boundary conditions for the BVP. In Phase II, near-surface hydrologic response for the C3 BVP was simulated with a variably saturated subsurface flow model, driven by both observed and hypothetical rainfall events. In Phase III, slope stability estimates for the C3 BVP were made using the infinite slope model, which was driven, in part, by the simulated pore pressures from Phase II.

Steady-state saturated subsurface flow simulations

The first model used in this study is the relatively simple NUM5 (R. A. Freeze, personal communication, 1981). As employed here, NUM5 is a 2D (vertical slice), steady-state, heterogeneous, saturated subsurface finite-difference flow model. The governing equation for NUM5 is:

$$\frac{\partial}{\partial y}\left[K_y(y,\,z)\frac{\partial h}{\partial y}\right]+\frac{\partial}{\partial z}\left[K_z(y,\,z)\frac{\partial h}{\partial z}\right]=0 \tag{1}$$

where K is the saturated hydraulic conductivity [LT^{-1}], h is the hydraulic head [L], and y and z [L] define the spatial domain. The solution to Equation 1 is $h(y, z)$. Hydraulic head is a fluid potential, with subsurface water moving in the direction of the maximum potential gradient.

Transient variably saturated subsurface flow simulations

The second model used in this study is VS2D (Lappala *et al*., 1993). As employed here, VS2D is a 2D (vertical slice), transient, heterogeneous, variably saturated subsurface finite-difference flow model. The governing equation for VS2D can be written as:

$$\frac{\partial}{\partial y}\left[K_y(F,\psi)\frac{\partial \psi}{\partial y}\right]+\frac{\partial}{\partial z}\left[K_z(F,\psi)\left(\frac{\partial \psi}{\partial z}+1\right)\right]=C(F,\psi)\frac{\partial \psi}{\partial t} \quad (2)$$

where $K(\psi)$ is the hydraulic conductivity function [LT^{-1}], F is the soil layer or geologic formation, ψ is the pressure head [L], $C(\psi)$ is the specific soil-water capacity function (i.e. slope of the soil-water retention curve, $d\theta/d\psi$) [–], θ is the soil-water content [–], and t is time [T]. The solution to Equation 2 is $\psi\,(y, z, t)$. The pressure head at a given location is related to the hydraulic head by $h = \psi + z$, where z is the elevation head [L]. Knowledge of either soil-water content or pressure head allows for the estimation of the other with an established soil-water retention curve.

Slope stability analysis

The slope stability analysis in this study is based upon the infinite slope model (see Selby, 1993), which can be expressed as:

$$FS=\frac{(c'+\Delta c)+[\gamma z'\cos^2\beta-p]\tan\phi'}{\gamma z'\sin\beta\cos\beta} \quad (3)$$

where FS is the factor of safety (i.e. the sum of resisting forces divided by the sum of driving forces) [–], c' is the intrinsic cohesion of the soil [$ML^{-1}T^{-2}$], Δc is the root cohesion [$ML^{-1}T^{-2}$], γ is the unit weight of the soil [$ML^{-2}T^{-2}$], z' is the depth from the surface to the shear plane [L], β is the slope angle [degrees], p is the pore water pressure [$ML^{-1}T^{-2}$], and ϕ' is the angle of internal friction [degrees]. Based on Equation 3, a slope is estimated to be unstable (subject to failure) when the value of FS is ≤1.

The application of the infinite slope model in this study is different from that typically reported, with separate FS estimates made along the failure plane, driven by individual pore pressures rather than a single average pore pressure. The relationship that links the variably saturated subsurface flow model (Equation 2) with the infinite slope model (Equation 3) is:

$$p=\rho g\psi \quad (4)$$

where ρ is the density of water at a standard temperature and pressure [ML^{-3}] and g is the acceleration due to gravity [LT^{-2}].

Boundary-value problems

WS3. The BVP for the simulations of WS3 with NUM5 is shown in Figure 2. The dimensions for the WS3 BVP are given in Table II. The region of flow, defined by the points A to D in Figure 2, represents a valley-centred heterogeneous vertical cross-section through the long profile, under fully saturated conditions. The location of the roadcut, along

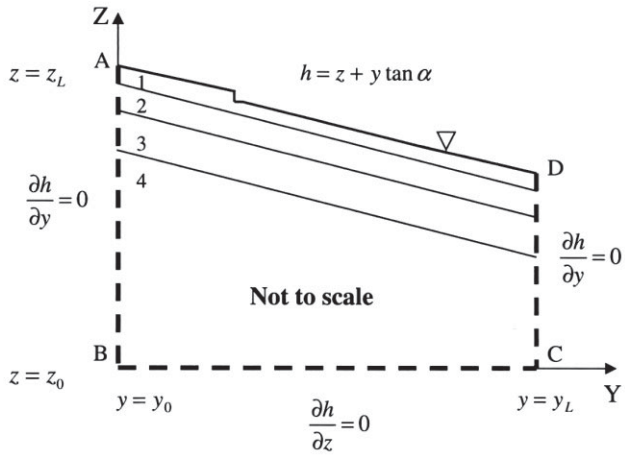

Figure 2. NUM5 representation of the WS3 BVP. The dimensions for the WS3 BVP are given in Table II.

Table II. Dimensions for the WS3 and C3 boundary-value problems

Characteristic	WS3 (see Figure 2)	C3 (see Figure 3)
z_0 (m)	0	0
z_L (m)	500	7
y_0 (m)	0	247
y_L (m)	1250	327
α (°)	20	30
Δy (m)	10	0·4
Δz (m)	2	0·05
Δt (s)	na	adaptive

Table III. Saturated hydraulic conductivity values used for the WS3 and C3 simulations

Unit*	Description	Depth† (m)	Saturated hydraulic conductivity (m s^{-1})	Source of saturated hydraulic conductivity value
1	A soil horizon	1·5	$1{\cdot}0 \times 10^{-3}$‡	Dutton (2000)
2	B soil horizon	1·5	$7{\cdot}0 \times 10^{-4}$§	Dutton (2000)
3	Saprolite	1.5	$1{\cdot}0 \times 10^{-6}$	Freeze and Cherry (1979)
4	Sandstone	na	$1{\cdot}0 \times 10^{-11}$	Freeze and Cherry (1979)
5	Road	0·95	$1{\cdot}0 \times 10^{-8}$	Loague and Kyriakidis (1997)

* See Figures 2 and 3.
† Dutton (2000).
‡ Average value from 36 measurements (Dutton, 2000).
§ Average value from 12 measurements (Dutton, 2000).

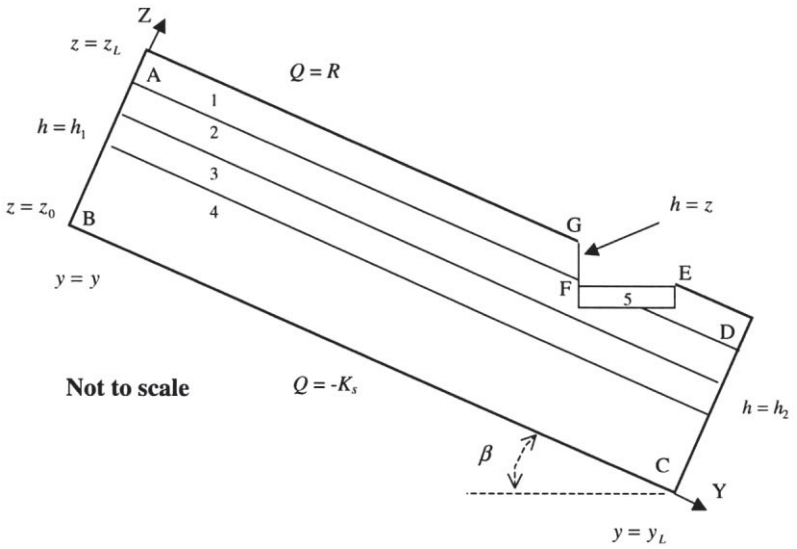

Figure 3. VS2D representation of the C3 BVP. The dimensions for the C3 BVP are given in Table II.

the long profile, is shown to the left of centre on the A–D boundary. The A–B, B–C, and C–D lines represent impermeable (no-flow) boundaries. The A–D line represents a water table boundary. The four layers of the grid represent the different soil and geologic units. The individual units in the layered slope were considered homogeneous and isotropic with respect to all soil and hydrogeologic parameters. Table III provides the saturated hydraulic conductivity values used for each of the four layers.

C3. The BVP for the simulations of C3 with VS2D is shown in Figure 3. The dimensions of the C3 BVP are given in Table II. The region of flow, defined by the points A to G in Figure 3, is a heterogeneous vertical cross-section

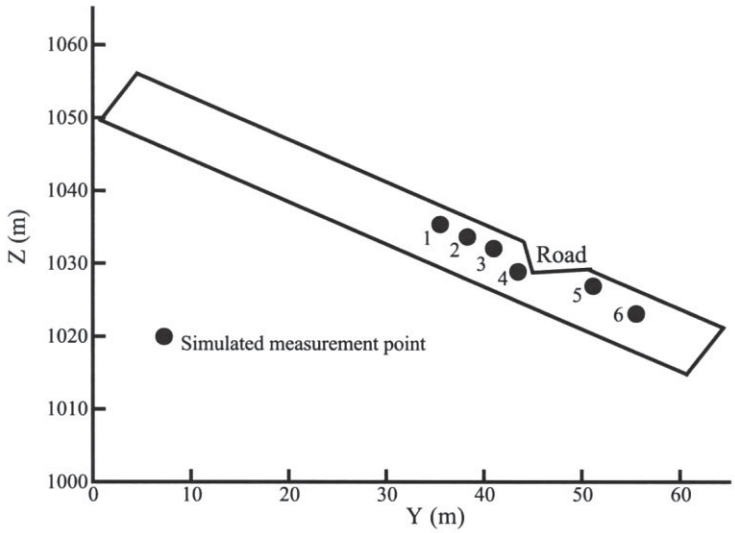

Figure 4. Locations of six near-surface simulated measurement points, relative to the road, for the C3 BVP.

through the long profile, under variably saturated conditions. The up-gradient boundary (A–B) was treated as a constant head; the surface boundary condition (A–D) was treated as a constant flux (flux rate equal to the rainfall rate); the boundary for the cutslope above the road (F–G) was treated as a seepage face; the boundary for road surface (E–F) was considered relatively impermeable (i.e. $K = 1{\cdot}0 \times 10^{-8}$ m s^{-1}); the down-gradient boundary (C–D) was treated as a constant head; the boundary at the base (B–C) was treated as a constant flux that leaked at a rate equal to the saturated hydraulic conductivity of the bedrock (i.e. unity gradient). Figure 4 shows the locations for six near-surface simulated measurement (i.e. pore pressure) points within the C3 BVP. It should be noted that the simulated measurement points are not located on the failure plane, but rather within the soil profile to illustrate the overall near-surface response (i.e. saturated versus unsaturated).

The individual units in the layered slope were considered homogeneous and isotropic with respect to all soil and hydrogeologic parameters. Table III provides the saturated hydraulic conductivity values used for each of the four layers and the road. The characteristic curve for soil-water retention (i.e. $\theta(\psi)$) developed for C3 (see Dutton, 2000) is typical of those reported for forested soils (e.g. Torres *et al*., 1998). The C3 soil-water retention curve was used to generate the hydraulic conductivity characteristic curve (i.e. $K(\psi)$; see Dutton, 2000), employing the van Genuchten (1980) approach. The soil-water content data obtained across C3 (see Dutton, 2000) did not exhibit any spatial structure. Therefore, the initial conditions (i.e. the pressure-head distribution) for simulations of C3 with VS2D were estimated by draining (by simulation) the saturated system until quasi-equilibrium was obtained. Once the pressure-head distribution is known, the water table location (i.e. $\psi = 0$) and the soil-water content distribution can be estimated.

The region of C3 susceptible to failure was represented as a rectangular soil block (of unit width) with uniform thickness and hydraulic properties. The soil block rests on a failure plane taken for this study to be at the permeability contrast between the soil and saprolite layers. Table IV provides the material property values used for the C3 slope stability analyses.

Table IV. Material property values used for the C3 slope stability estimates

Parameter	Symbol	Value	Source
Failure plane slope	β	30°	Dutton (2000)
Effective cohesion of the soil	c'	1·5 kN m^{-2}	Selby (1993)
Root cohesion	Δc	5 kN m^{-2}	Selby (1993)
Unit weight of soil	γ	19·6 kN m^{-3}	Selby (1993)
Depth from surface to the failure plane	z'	3 m	Dutton (2000)
Angle of internal friction	ϕ'	20°	Selby (1993)

Results

Phase I

The simulated subsurface flow field for the WS3 BVP shown in Figure 2 has, as one should expect (i.e. Toth, 1963), an up-slope region of recharge and down-slope region of discharge. The steady-state, fully saturated simulation is characterized by near-surface groundwater movement parallel to the surface through the high permeability soil above the saprolite contact (see Dutton, 2000). It is important to note that the impact of the road on subsurface flow was only felt within the near-surface at a local scale (see Dutton, 2000). Therefore, it was possible, as intended, to use the results from WS3 simulation to set the dimensions (e.g. depth) and up- and down-gradient boundaries for the C3 BVP (see Figure 3 and Table II).

Phase II

The simulated subsurface flow results for the C3 BVP shown Figure 3 are presented in two parts. In the first part, three observed rainfall events are considered; in the second part, a hypothetical rainfall event is considered with two scenarios for the initial pressure-head distribution.

Three observed rainfall events. The drainage simulations for the C3 BVP with VS2D, conducted to estimate an internally valid pressure-head distribution, set the water table approximately 2 m below the surface. The summary characteristics of the three 1996 rainfall events are given in Table V. It should be pointed out that the real-time intensity varies during the course of each rainfall event (see Dutton, 2000). The results (in terms of hydraulic head) from each of the observed rainfall simulations show that subsurface flow paths, in the area of the road, are diverted upward toward the seepage face in the near-surface and dip beneath the compacted soil (i.e. out of the BVP) at greater depth (see Dutton, 2000). These findings should be expected based upon, for example, the Rulon *et al*. (1985) conclusions concerning the location, geometry, and magnitude of near-surface permeability contrasts. In that no pressure head data were available for the three C3 rainfall events, the representativeness of the subsurface flow simulations to actual conditions is evaluated by comparing (see Figure 5) the observed and simulated seepage discharges at the roadcut face. Figure 5 shows that (i) the observed versus simulated discharges match well for all three events and (ii) the overall response, with the same initial conditions, is greater for the larger events. It should be

Table V. Characteristics of three observed (1996) C3 rainfall events

Date (month/day)	Depth (mm)	Average intensity (mm hr^{-1})	Duration (days)
11/24	103	1·5	*c.* 1·5
11/29	51	2·5	*c.* 3·5
12/28	165	2·6	*c.* 4·0

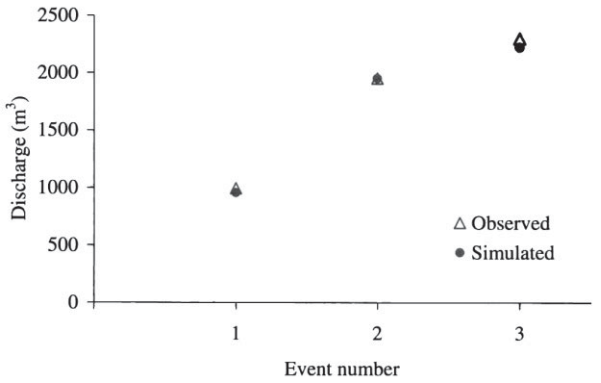

Figure 5. Comparison of observed and simulated discharge at the C3 roadcut face for three 1996 events: 1, 24 November; 2, 29 November; 3, 28 December

Table VI. VS2D simulated pore pressures used in the *FS* estimates for Scenarios A and B

	Pore pressure (Pa)					
Scenario	**Point 1***	**Point 2**	**Point 3**	**Point 4**	**Point 5**	**Point 6**
A	10 270	10 496	10 917	921	−17 738	−8778
B	15 543	14 259	12 711	1078	−17 581	−8560

* See Figure 4 for the locations of the simulated measurement points.

pointed out that the height of the seepage face used to determine the discharge through the roadcut face was a trial-and-error best-fit approximation. The success in simulating the three observed events establishes a foundation for simulations with a large intensity hypothetical rainfall event described in the next section.

Hypothetical rainfall event, scenarios A and B. A hypothetical rainfall event was used for concept-development simulations of near-surface hydrologic response and slope stability. To test the stability of the C3 slope above the roadcut, a shorter but more intense (relative to the three 1996 observed events) hypothetical event was considered. The constant intensity for the 24-hour hypothetical event was set at 3·6 mm h^{-1}. Two initial water table position scenarios were considered for the hypothetical rainfall event: for Scenario A the water table was approximately 2 m below the surface; for Scenario B the water table was approximately 1 m below the surface. Table VI lists simulated pore pressure values (at the measurement points shown in Figure 4) for both scenarios 24 hours after the end of the hypothetical rainfall event.

The simulated characterization of subsurface response for Scenarios A and B are generally (albeit with higher resulting water tables and larger seepage discharges) the same as described for the three observed events (i.e. flow paths diverge, relative to depth, either upward toward the seepage face or downward beneath the road). Inspection of Table VI (with reference to the measurement point locations given in Figure 4) shows that the simulated pore pressures are positive (saturated conditions) up-slope of the road and negative (unsaturated conditions) below the road for both scenarios. Further inspection of the results in Table VI shows that the difference between the two scenarios is twofold: (i) up-slope of the road (i.e. points 1 to 4) the pore pressures are greater (more positive) for Scenario B (i.e. higher water table) and (ii) down-slope of the road (i.e. points 5 and 6) the pore pressures are smaller (more negative) for Scenario A (i.e. lower water table).

Phase III

The C3 slope stability estimates are presented in three parts. The first part is driven by the results from the subsurface flow simulations for the three observed rainfall events (reported in part one of Phase II). The second part is driven by the results from the subsurface flow simulations for the hypothetical rainfall event with two initial pressure-head distribution scenarios (reported in part two of Phase II). The third part is a sensitivity analysis with Scenario A (from part two of Phase II) taken as the base case. It should be pointed out that the *FS* results presented here (i.e. Figures 6 to 8) are between the 30 and 50 m *x*-axis coordinates shown in Figure 4. The focus on this 20 m section of the failure plane is based upon: (i) the study objective to investigate if a near-surface permeability contrast (associated with forest road) can lead to slope failure directly up-slope of the road, and (ii) a desire to minimize the effects of the up- and down-gradient boundary conditions in the VS2D simulations of pressure head. It should also be pointed out that the *FS* estimates shown in Figures 6 to 8 are based upon linear interpretations of pore pressures determined from simulated pressure heads at nodal sites (within the finite-difference grid) along the failure plane.

Three observed rainfall events. Employing the simulated pore pressure results from the first part of Phase II, *FS* analyses were performed 24 hours after the end of each event with Equation 3 for the three observed C3 rainfall events. Figure 6 shows the results from the three *FS* analyses. Inspection of Figure 6 shows that *FS* is greater than 1·0 along the entire length of the failure plane. According to the results from the subsurface flow simulations (i.e. pore pressures), the results in Figure 6 should be expected, as C3 did not fail above the road for any of the three 1996 events. Two important features from the results in Figure 6 are (i) the decrease in *FS* values just above and at the road, and (ii) the sharp increase in *FS* values below the road. The overall differences between the *FS* estimates shown in Figure 6 are attributed to the individual characteristics of the three events (e.g. time series of rainfall intensity).

Hypothetical rainfall event, scenarios A and B. Employing pore pressure simulated at the failure plane, *FS* analyses were performed 24 hours after the end of the hypothetical rainfall event with Equation 3 for the two initial water table position scenarios. The reader is reminded that the approximate initial position of the water table below the surface is

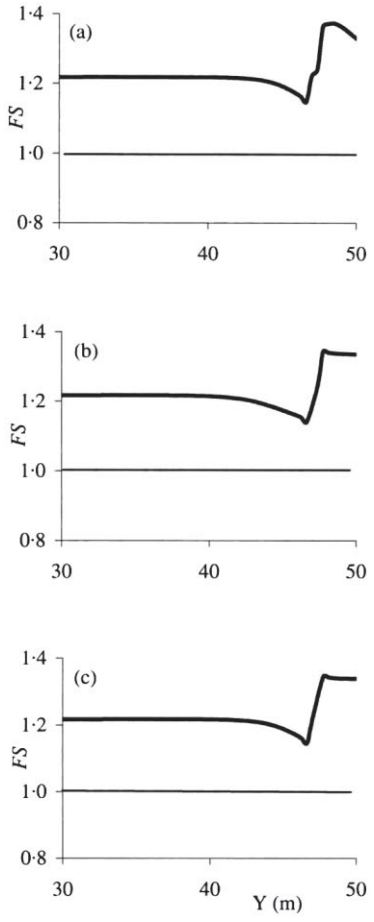

Figure 6. Factor of safety estimates for the C3 BVP for the three observed rainfall events from 1996 (i.e. 24 hours after the end of each event): (a) 24 November; (b) 29 November; (c) 28 December. The location of the road is shown in Figure 4; the *FS* = 1·0 line is shown for reference.

2 m for Scenario A and 1 m for Scenario B. The reader is also reminded that the pore pressures given in Table VI are from within the soil profile (i.e. not at the failure plane).

The *FS* results for Scenarios A and B are given in Figure 7. Figure 7a (Scenario A) and b (Scenario B) show that in the area of the road the *FS* values are less than 1·0 (i.e. predicted slope failure), due to the high pore pressures associated with the subsurface flow field being diverted upward toward the seepage face. The effect of the initial water table position is shown in Scenario B (as compared to Scenario A) where the *FS* values are less than 1·0 along the entire failure plane. It is also clearly shown in Figure 7, for both scenarios, that there is a dramatic increase in the *FS* values downslope of the road, resulting from lower pore pressures (e.g. see points 5 and 6 in Table VI) associated with the subsurface flow field dipping beneath the road. The greater potential for slope failure for the hypothetical rainfall event (see Figure 7), compared to the observed rainfall events (see Figure 6), is due to the long duration of constant high intensity rainfall, resulting in the build-up of pore pressures (see Table VI).

Sensitivity of the FS *estimates for the hypothetical rainfall event, scenario A.* A reasonable set of parameter values was selected for the C3 *FS* calculations in this study (see Table IV). There is of course uncertainty associated with some of these values relative to the *FS* estimates for C3. Figure 8 shows the impact, relative to the Scenario A base case (see Figure 7a), of varying (individually) five of the values in Table IV by ±10 per cent for the C3 BVP for the hypothetical rainfall event. The variables considered in Figure 8 are: z' (depth of the failure plane; Figure 8a); Δc (root cohesion; Figure 8b); β (slope angle; Figure 8c); ϕ' (internal angle of friction; Figure 8d); and c' (intrinsic soil cohesion; Figure 8e). Inspection of Figure 8 shows that up-slope of the road, the *FS* values are, in comparison to the base case, lower (i.e. less stable slope), as should be expected, for +10 per cent changes in z' and β and −10 per cent changes in Δc, ϕ', and c'. For each of the less stable cases, with the exception of intrinsic soil cohesion, the *FS* values

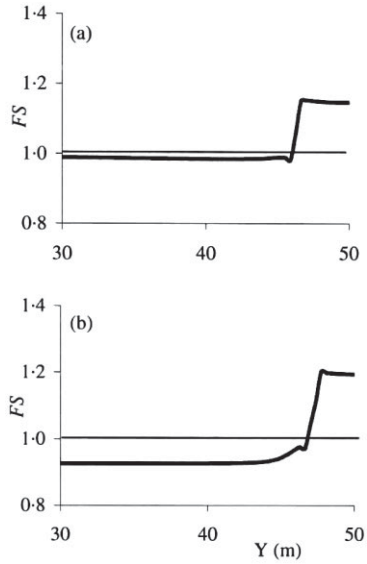

Figure 7. Factor of safety estimates for the C3 BVP for the hypothetical rainfall event (i.e. 24 hours after the end of the rainfall event): (a) Scenario A; (b) Scenario B. The location of the road is shown in Figure 4; the *FS* = 1·0 line is shown for reference.

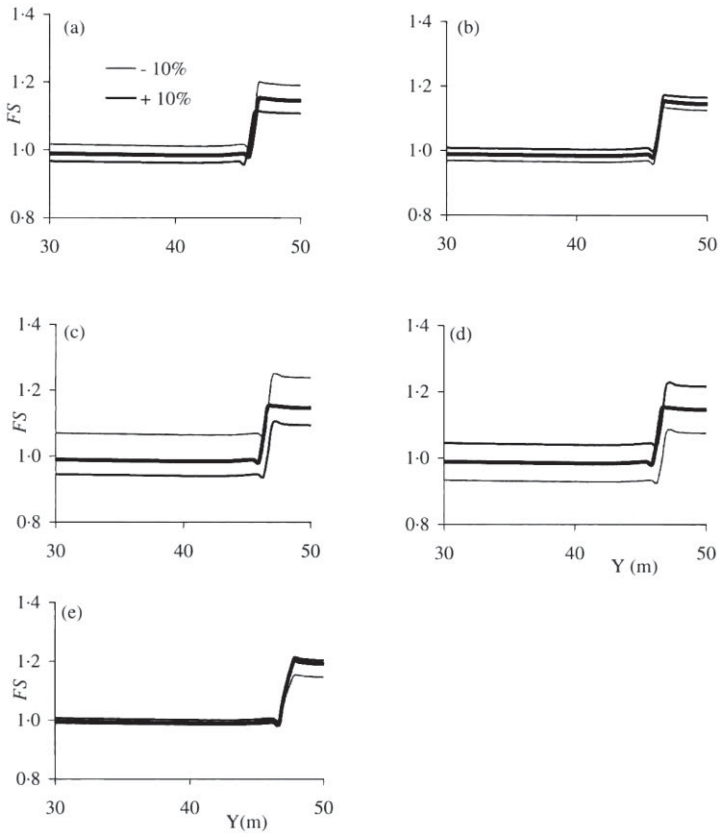

Figure 8. Plus and minus 10 per cent sensitivity analysis results for C3 estimates of *FS*: (a) *z*, depth of failure plane; (b) Δc, root cohesion; (c) β, slope angle; (d) ϕ', angle of internal friction; (e) c', intrinsic soil cohesion. The base case (shown in bold) is Scenario A shown in Figure 7a. The location of the road is shown in Figure 4.

are lower than 1·0 for the entire failure plane, as seen for the higher water table in Scenario B (see Figure 7b). Careful inspection of Figure 8 shows that the impact on the *FS* estimates, relative to the ±10 per cent changes in the parameter values, is significantly greater for β and ϕ' than for z', Δc, and c'.

Discussion

Wemple and Jones (2003; also see Wemple, 1998) have addressed the effect of the forest road at C3 using both field data and simulation. The subsurface stormflow simulations of Wemple and Jones (2003), although not specifically focused on slope stability, and the effort reported here both show that the C3 forest road plays an important role in governing near-surface hydrologic response as it is related to up-slope failures. Several authors have discussed the use of subsurface (both saturated and variably saturated) flow models to determine pore pressures for slope stability analysis (e.g. Hodge and Freeze, 1977; Rulon and Freeze, 1985; Reid and Iverson, 1992). To the best of our knowledge this is the first attempt to link a variably saturated subsurface flow model (based on potential theory) to a slope stability analysis for the forest road BVP. The effort reported here illustrates that for near-surface systems, with transient water tables responding to individual rainfall events, rigorous assessment of unsaturated/saturated subsurface flow is needed to make quantitative pore pressure estimates. It is important to acknowledge that simulations of the type reported here for C3 need to be evaluated based upon field observations well beyond the limited roadcut seepage discharge comparisons made in this study. The spatial and temporal distributions of pressure head and soil-water content need to be measured for a more rigorous assessment of model performance.

The effort report here sets a foundation for future modelling efforts focused on capturing the 3D effects of near-surface hydrologic response for steep incised hillslopes that are dissected by a road. Relative to the VS2D simulated pore pressures, the slope stability estimates reported here for C3 are almost certainly conservative. The fact that the subsurface flow for the C3 site was simulated as a 2D long profile vertical slice neglects the important lateral flow component of the system. For example, characterization of convergent lateral subsurface flow for the C3 site would almost certainly result in (relative to the estimates in this study) increased pore pressures and, therefore, decreased slope stability.

Based upon recent developments, future physics-based simulation (see Loague and VanderKwaak, 2004) efforts will be designed to characterize more than a single hydrologic-response process. Related to the problem focused on in this study, concept-development simulations considering the effect that a forest road can have on slope stability (both above and below the road), as well as erosion from surface runoff (on the road), is a near-surface BVP well within reach, given sufficient data. For example, the integrated hydrology model (I*n*HM) developed by VanderKwaak (1999) was designed to simulate first-order coupled 3D variably saturated subsurface flow and 2D flow over the surface and in channels. I*n*HM is fully capable of simulating the four streamflow-generation mechanisms (i.e. Dunne and Horton overland flow, subsurface stormflow, groundwater), thereby facilitating simultaneous characterization of the total hydrologic response needed for the assessment of slope stability. It is worth pointing out that I*n*HM has been successfully employed for a rangeland catchment with ranch roads (e.g. VanderKwaak and Loague, 2001; Loague and VanderKwaak, 2002; Loague *et al*., in press).

The relatively simple application of the infinite slope model in this study is for separate *FS* estimates (driven by individaul pore pressures) along the failure plane. It is important to clarify that only the initiation of slope failure is considered in this study. In the future it may be possible (given sufficient data) to employ the linear elastic deformation equations (e.g. Iverson and Reid, 1992a, b), with pore pressures estimated via fully coupled 3D near-surface variably saturated hydrologic-response simulation, to assess the initiation of slope failure at the hillslope scale (including the road problem).

Conclusions

The results reported here for the C3 site support the hypothesis that a near-surface permeability contrast, caused by the surface compaction associated with forest roads, can result in diverted subsurface flow paths that produce increased up-slope pore pressures, resulting in slope failure. The permeability contrast associated with the C3 forest road was shown, via simulation with a variably saturated subsurface flow model responding to event-based rainfall, to alter slope-parallel subsurface flow, resulting in increased pore pressures up-gradient of the road, which in turn led to predictions with the infinite slope model of slope failure for high intensity rainfall. The effort reported here is a foundation step for considering the effects that a forest road can have on near-surface hydrologic response and slope stability.

Acknowledgments

This study could not have been undertaken without the permission and generous cooperation of the folks at the H. J. Andrews Experimental Forest, especially Fred Swanson, Julia Jones and Reed Perkins. The various contributions of Leigh Soutter, Mike Pinto, and Iris Stewart are greatly appreciated. The computing facilities used in this study were provided by an equipment grant from the National Science Foundation. The field work at the HJA was supported, in part, by National Science Foundation Grants DEB-96-32921 and BSR-90-11663. The effort reported here is a Center for Earth Science Information Research (CESIR) contribution.

References

Beschta RL. 1978. Long-term patterns of sediment production following road construction and logging in the Oregon Coast Range. *Water Resources Research* **14**: 1011–1016.

Beven K. 1982. On subsurface stormflow: Predictions with simple kinematic theory for saturated and unsaturated flows. *Water Resources Research* **18**: 1627–1633.

Bilby RE, Sullivan K, Duncan SH. 1989. The generation and rate of road-surface sediment production in forested watersheds in southwestern Washington. *Water Resources Research* **14**: 1011–1016.

Bowling LC, Lettenmaier DP. 2001. The effects of forest roads and harvest on catchment hydrology in a mountainous maritime environment. In *Land Use and Watersheds: Human Influence on Hydrology and Geomorphology in Urban and Forest Areas*, Wigmosta MS, Burges SJ (eds). Water and Science Application, Volume 2. American Geophysical Union: Washington, DC; 145–164.

Brown GW, Krygier JT. 1971. Clear-cut logging and sediment production in the Oregon Coast Range. *Water Resources Research* **7**: 1189–1198.

Dhakal AK, Sidle RC, Wu W. 2000. Integrating the hydrologic effects of forest roads into a distributed slope stability model. *EOS, Transactions, American Geophysical Union* **81**: F487.

Duan J. 1996. *A coupled hydrologic-geomorphic model for evaluating effects of vegetation change on watersheds*. PhD dissertation, Oregon State University.

Dutton AL. 2000. *Process-based simulations of near-surface hydrologic response for a forested upland catchment: The impact of a road*. MS thesis, Stanford University, Stanford, California.

Dyrness CT. 1967. *Mass soil movements in the HJ Andrews Experimental Forest*. PNW-42. Pacific Northwest Forest and Range Experiment Station. USDA, USFS.

Fisher JC. 2000. *Simulation of partially saturated – saturated flow in the Caspar Creek E-road groundwater system*. MS thesis, Humboldt State University, Arcata, California.

Freeze RA, Cherry JA. 1979. *Groundwater*. Prentice Hall: Englewood Cliffs, New Jersey.

Harr RD. 1977. Water flux in soil and subsoil on a steep forested slope. *Journal of Hydrology* **33**: 37–58.

Harr RD, Harper WC, Krygier JT, Hsieh FS. 1975. Changes in storm hydrographs after road building and clear-cutting in the Oregon Coast Range. *Water Resources Research* **11**: 436–444.

Hodge RA, Freeze RA. 1977. Groundwater flow systems and slope stability. *Canadian Geotech Journal* **14**: 466–476.

Iverson RM, Reid ME. 1992a. Gravity-driven groundwater flow and slope failure potential. 1. Elastic effective stress model. *Water Resources Research* **28**: 925–938.

Iverson RM, Reid ME. 1992b. Gravity-driven groundwater flow and slope failure potential. 2. Effects of slope morphology, material properties, and hydraulic heterogeneity. *Water Resources Research* **28**: 939–950.

Jones JA, Grant GE. 1996. Peak flow responses to clear-cutting and roads in small and large basins, Western Cascades, Oregon. *Water Resources Research* **32**: 959–974.

King JG, Tennyson LC. 1984. Alteration of streamflow characteristics following road construction in North Central Idaho. *Water Resources Research* **20**: 1159–1163.

Lappala EG, Healy RW, Weeks EP. 1993. *Documentation of computer program VS2D to solve the equations of fluid flow in variably saturated porous media*. Water Resources Investigation Report 83-4099, USGS Open File Reports.

Loague K, Kyriakidis PC. 1997. Spatial and temporal variability in the R-5 infiltration data set: Deja vu and rainfall-runoff simulations. *Water Resources Research* **33**: 2883–2895.

Loague K, VanderKwaak JE. 2002. Simulating hydrologic response for the R-5 catchment: Comparison of two models and the impact of the roads. *Hydrological Processes* **16**: 1015–1032.

Loague K, VanderKwaak JE. 2004. Physics-based hydrologic response simulation: Platinum bridge, 1958 Edsel, or useful tool. *Hydrological Processes* **18**: 2949–2956.

Loague K, Heppner CS, Abrams RH, VanderKwaak JE, Carr AE, Ebel BA. In press. Further testing of the Integrated Hydrology Model (InHM): Event-based simulations for a small rangeland catchment located near Chickasha, Oklahoma. *Hydrological Processes*.

Luce CH, Cundy TW. 1994. Parameter identification for a runoff model for forest roads. *Water Resources Research* **30**: 1057–1069.

Luce CH, Wemple BC (eds). 2000. Special issue: Hydrologic and geomorphic effects of forest roads. *Earth Surface Processes and Landforms* **26**: 111–232.

Megahan WF, Clayton JL. 1983. Tracing subsurface flow on roadcuts on steep, forested slopes. *Soil Science Society of America* **47**: 1063–1067.

Reid LM, Dunne T. 1984. Sediment production from forest road surfaces. *Water Resources Research* **20**: 1753–1761.

Reid ME. 1997. Slope instability caused by small variation in hydraulic conductivity. *Journal of Geotechnical and Geoenvironmental Engineering* **123**: 717–725.

Reid ME, Iverson RM. 1992. Gravity driven groundwater flow and slope failure potential, 2. Effects of slope morphology, material properties, and hydraulic heterogeneity. *Water Resources Research* **28**: 939–950.

Rulon JJ, Freeze RA. 1985. Multiple seepage faces on layered slopes and their implications for slope stability analysis. *Canadian Geotechnical Journal* **22**: 347–356.

Rulon JJ, Rodway R, Freeze RA. 1985. The development of multiple seepage faces on layered slopes. *Water Resources Research* **21**: 1625–1636.

Selby MJ. 1993. *Hillslope Materials and Properties*. Oxford University Press: New York.

Swanson FJ, Dyrness CT. 1975. Impact of clear-cutting and road construction on soil erosion by landslides in the western Cascade Range, Oregon. *Geology* **3**: 393–396.

Tague C, Band L. 2001. Simulating the impact of road construction and forest harvesting on hydrologic response. *Earth Surface Processes and Landforms* **26**: 135–151.

Thomas RB, Megahan WF. 1998. Peak flow response to clear-cutting and roads in small and large Basins, Western Cascades, Oregon: A second opinion. *Water Resources Research* **34**: 3393–3403.

Toth J. 1963. A theoretical analysis of groundwater flow in small drainage basins. *Journal of Geophysical Research* **68**: 4795–4812.

Torres R, Dietrich WE, Montgomery DR, Anderson SP, Loague K. 1998. Unsaturated zone processes and the hydrologic response of a steep, unchanneled catchment. *Water Resources Research* **34**: 1865–1879.

van Genuchten MTh. 1980. A closed-form equation for predicting the hydraulic conductivity of unsaturated soils. *Soil Science Society of America* **44**: 892–898.

VanderKwaak JE. 1999. *Numerical simulation of flow and chemical transport in integrated surface-subsurface hydrologic systems*. PhD dissertation, University of Waterloo, Waterloo, Ontario, Canada.

VanderKwaak JE, Loague K. 2001. Hydrologic-response simulations for the R-5 catchment with a comprehensive physics-based model. *Water Resources Research* **37**: 999–1013.

Wemple BC. 1998. *Investigations of runoff production and sedimentation on forest roads*. PhD dissertation. Oregon State University, Corvallis, Oregon.

Wemple BC, Jones JA. 2003. Runoff production on forest roads in a steep, mountain catchment. *Water Resources Research* **39**(SWC8): 1220. DOI:10.1029/2002WR001744

Wemple BC, Swanson FJ, Jones JA. 2001. Forest roads and geomorphic interactions, Cascade Range, Oregon. *Earth Surface Processes and Landforms* **26**: 191–204.

Wigmosta MS, Perkins WA. 2001. Simulating the effects of forest roads on watershed hydrology. In *Land Use and Watersheds: Human Influence on Hydrology and Geomorphology in Urban and Forest Areas*, Wigmosta MS, Burges SJ (eds). Water and Science Application, Volume 2. American Geophysical Union: Washington, DC; 127–143.

Ziegler AD, Giambelluca TW, Sutherland RA. 2001. Erosion prediction on unpaved mountain roads in northern Thailand: Validation of dynamic erodibility modelling using KINEROS2. *Hydrological Processes* **15**: 337–358.

Ziemer RR. 1981. Storm flow response to road building and partial cutting in small streams of Northern California. *Water Resources Research* **17**: 907–917.

